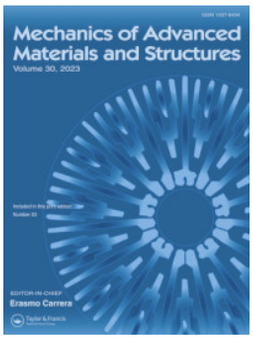

Taylor & Francis
Taylor & Francis Group

Mechanics of Advanced Materials and Structures

ISSN: (Print) (Online) Journal homepage: https://www.tandfonline.com/loi/umcm20

Nonlinear inertial amplifier resilient friction base isolators for multiple degrees of freedom systems

Sudip Chowdhury, Arnab Banerjee & Sondipon Adhikari

To cite this article: Sudip Chowdhury, Arnab Banerjee & Sondipon Adhikari (21 Sep 2023): Nonlinear inertial amplifier resilient friction base isolators for multiple degrees of freedom systems, Mechanics of Advanced Materials and Structures, DOI: 10.1080/15376494.2023.2257433

To link to this article: https://doi.org/10.1080/15376494.2023.2257433

MECHANICS OF ADVANCED MATERIALS AND STRUCTURES
https://doi.org/10.1080/15376494.2023.2257433

Taylor & Francis
Taylor & Francis Group

ORIGINAL ARTICLE

Nonlinear inertial amplifier resilient friction base isolators for multiple degrees of freedom systems

Sudip Chowdhury[a], Arnab Banerjee[a], and Sondipon Adhikari[b]

[a]Civil Engineering Department, Indian Institute of Technology, Delhi, India; [b]James Watt School of Engineering, The University of Glasgow, Glasgow, Scotland, United Kingdom

ABSTRACT

This study introduces the nonlinear inertial amplifier resilient friction bearing isolators (NIARFBI). Another friction base isolator, namely the nonlinear inertial amplifier friction pendulum system (NIAFPS), is derived by eliminating the static damping from the governing equation of motion of the NIARFBI. The damping for NIAFPS is generated through the motion of the friction element of the isolator during the movement of the base layer. These novel isolators are placed at the base of the multiple degrees of freedom (MDOF) systems to reduce their dynamic responses. Every element of the highly nonlinear governing equations of motion of the dynamic systems isolated by each nonlinear isolator is linearized using the stochastic linearization approach. The specific mathematical formulation for the optimal design parameters for each nonlinear isolator is derived using the H_2 optimization approach. In order to determine the dynamic responses analytically, the transfer function is established. The dynamic responses of the novel isolators are compared with the dynamic responses of the traditional isolators. Accordingly, the displacement reduction capacities of optimum NIARFBI and NIAFPS are significantly 93.60% and 70.82%, superior to TRFBI and TFPS. The acceleration reduction capacities of optimum NIARFBI and NIAFPS are 88.27% and 58.92% superior to TRFBI and TFPS. The recently developed expressions for this study are all mathematically accurate and applicable for practical applications.

ARTICLE HISTORY
Received 28 July 2023
Accepted 2 September 2023

KEYWORDS
Traditional friction pendulum systems (TFPS); traditional resilient friction base isolators (TRFBI); nonlinear inertial amplifier resilient friction bearing isolators (NIARFBI); nonlinear inertial amplifier friction pendulum system (NIAFPS); H_2 optimization approach

1. Introduction

Base isolation [1], also known as seismic isolation or earthquake isolation, is a structural engineering technique used to protect buildings and other structures from the damaging effects of earthquakes [2]. The primary objective of base isolation is to decouple the superstructure (the building or structure above ground) from the ground motion generated by an earthquake, thereby reducing the transmission of seismic forces and preventing excessive lateral movement and shaking [3]. Elastomeric bearings [4], sliding bearings [5], laminated rubber bearings [6], lead rubber bearings [7], inerter-based isolators [8], and inertial amplifier-based isolators [9] are one of the base isolation systems [10–12] applied to the dynamic systems to control the dynamic responses subjected to earthquake excitations.

To achieve the robust dynamic response reduction capacity from these isolators, the design parameters need to be optimized. H_2 optimization method is one of the prominent analytical optimization methods. Using this method, the optimal design parameters can be derived in terms of closed-form expressions [13]. This method is applicable for randomly excited isolated structures. Another method to achieve robust vibration reduction performance from isolators is to increase their static mass, which over-increases the flexibility of the base layer during seismic events. In addition, the base isolator is not well performed for high-rise buildings. Therefore, to reduce these drawbacks, instead of static mass, the effective mass of the isolators is trying to increase using inerters [14, 15] and inertial amplifiers. An inerter, also known as an inertance device or dynamic vibration absorber, is a mechanical component used in engineering and vehicle suspension systems. It was introduced in the early 2000s as a potential improvement to vehicle suspension systems [16]. The inerter's [17, 18] purpose is to provide additional damping by increasing the isolation systems' effective mass. The key characteristic of an inerter is that its force is proportional to the relative acceleration between its ends. This means that the inerter generates a force that opposes this relative motion, thus providing additional damping. Inertial amplifiers [19, 20] are also one of the effective mass amplification devices which can increase effective mass, damping of the isolation systems. It can also provide additional flexibility with sufficient load-bearing capacity simultaneously to the isolators during seismic events. Therefore, the base layer of the isolators may not be damaged, and the time period of the isolated structures may increase. Both inerters and inertial amplifier based isolators are applicable to high rise buildings. However, to increase the reliability and performance of the enhanced isolators, the inertial amplifiers are induced inside the core materials of the nonlinear isolators, such as resilient friction base isolation (RFBI) and friction pendulum systems (FPS). The application of inertial amplifiers to RFBI and FPS for mitigating the dynamic

CONTACT Sudip Chowdhury sudip.chowdhury@civil.iitd.ac.in Civil Engineering Department, Indian Institute of Technology, Delhi, India

responses of the multiple degrees of freedom systems [21] and their corresponding analytical closed-form expressions for optimal design parameters do not exist in state of the art. Therefore, a research gap is identified.

To address the research gap, the nonlinear inertial amplifier resilient friction base isolation (NIARFBI) and nonlinear inertial amplifier friction pendulum systems (NIAFPS) are introduced in this paper. These isolators are applied to multiple degrees of freedom systems (MDOF) to mitigate their dynamic responses. H_2 optimization method is applied to derive the mathematical formulations for optimal design parameters for NIARFBI and NIAFPS applied to multiple degrees of freedom systems. The dynamic responses of the NIARFBI and NIAFPS-controlled MDOF systems are compared with the traditional resilient friction base isolation (TRFBI) and traditional friction pendulum systems (TFPS)-controlled MDOF systems to obtain the superior dynamic response reduction capacity (%) of NIARFBI and NIAFPS.

2. Structural model and equations of motion

Figure 1(a) displays the multiple degrees of freedom systems are isolated by NIARFBI and NIAFPS, where m_b, c_b, k_b, and μ state the static mass, damping, stiffness, and Poisson's ratio of for both isolators. m_a and θ state the amplifier's mass and inertial angle. The mass, damping, and stiffness of each floor are considered the same, i.e. $m_1 = m_{N-1} = m_N = m_s, k_1 = k_{N-1} = k_N = k_s,$ and $c_1 = c_{N-1} = c_N = c_s$. The governing equations of motion of MDOF systems isolated by NIARFBI and NIAFPS are derived using Lagrange's equations and expressed as

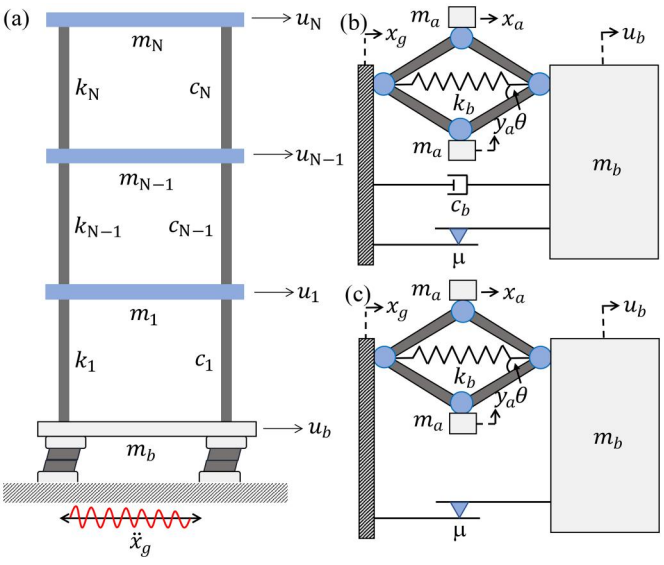

Figure 1. (a) The multi-degrees-of-freedom systems isolated by NIARFBI and NIAFPS. (b) The schematic diagrams of NIARFBI and NIAFPS.

$$
\begin{aligned}
&[\boldsymbol{M}_s]\{\ddot{x}_s\} + [\boldsymbol{C}_s]\{\dot{x}_s\} + [\boldsymbol{K}_s]\{\boldsymbol{x}_s\} = -[\boldsymbol{M}_s]\{\boldsymbol{r}\}(\ddot{x}_g + \ddot{x}_b)\\
&m_d\ddot{x}_b + c_d\dot{x}_b + k_d x_b + \mu m_d g\,\mathrm{sgn}(\dot{x}_b) - c_1\dot{x}_1 - k_1 x_1 = -m_d\ddot{x}_g\\
&m_d\ddot{x}_b + k_d x_b + \mu m_d g\,\mathrm{sgn}(\dot{x}_b) - c_1\dot{x}_1 - k_1 x_1 = -m_d\ddot{x}_g
\end{aligned}
\tag{1}
$$

where m_d, c_d, and k_d state the effective mass, damping, and stiffness of NIARFBI and NIAFPS; $m_d = m_b + 0.5m_a\left(1 + \frac{1}{2\tan^2\theta}\right)$. The statistical linearization method [8, 22] applies to Eq. (1) and linearized equation of motion are obtained. To perform that, it has been considered that the isolated structures are subjected to random white noise excitations having zero mean [23]. The friction element inside friction isolators provides additional damping to the nonlinear friction-based isolators. To apply the H_2 optimization method for achieving optimal design parameters in terms of closed-form expressions, the nonlinear damping part with the signum function has been linearized.

$$
c_e = E\left\{\frac{\partial(\mu m_d g\,\mathrm{sgn}(\dot{x}_b))}{\partial\dot{x}_b}\right\} = \sqrt{\frac{2}{\pi}}\frac{\mu m_d g}{\sigma_{\dot{x}_b}} \tag{2}
$$

$$
\begin{aligned}
&m_d\ddot{x}_b + k_d x_b + (c_d + c_e)\dot{x}_b - c_1\dot{x}_1 - k_1 x_1 = -m_d\ddot{x}_g\\
&m_d\ddot{x}_b + k_d x_b + c_e\dot{x}_b - c_1\dot{x}_1 - k_1 x_1 = -m_d\ddot{x}_g\\
&c_e = \sqrt{\frac{2}{\pi}}\frac{\mu m_d g}{\sigma_{\dot{x}_b}} \quad \text{and} \quad \mu_d = \mu_b + 0.5\mu_a\left(1 + \frac{1}{2\tan^2\theta}\right)
\end{aligned}
\tag{3}
$$

The steady-state solutions are applied to the governing equations of motion for generating the transfer function, i.e. $x_s = X_s e^{i\omega t}, x_b = X_b e^{i\omega t},$ and $\ddot{x}_g = X_g e^{i\omega t}$. The velocity responses are derived as $\dot{x}_s = (i\omega)X_s e^{i\omega t}, \dot{x}_b = (i\omega)X_b e^{i\omega t}$ and the acceleration responses are derived as $\ddot{x}_s = -\omega^2 X_s e^{i\omega t}, \ddot{x}_b = -\omega^2 X_b e^{i\omega t}$. $(\bullet)^{\cdot}$ defines the derivative with respect to time.

$$
\begin{bmatrix}
V_1 & V_2 & 0 & 0 & 0 & q^2\\
V_2 & V_1 & V_2 & 0 & 0 & q^2\\
0 & V_2 & V_1 & V_2 & 0 & q^2\\
0 & 0 & V_2 & V_1 & V_2 & q^2\\
0 & 0 & 0 & V_2 & V_3 & q^2\\
V_2 & 0 & 0 & 0 & 0 & V_4
\end{bmatrix}
\begin{Bmatrix} X_1\\ X_2\\ X_3\\ X_4\\ X_5\\ X_b \end{Bmatrix}
= -\begin{bmatrix} 1\\ 1\\ 1\\ 1\\ 1\\ \mu_d \end{bmatrix} X_g \tag{4}
$$

$$
\begin{aligned}
&q = i\omega, V_1 = 4\ \zeta_s q\omega_s + q^2 + 2\ \omega_s{}^2, V_2 = -2\ \zeta_s q\omega_s - \omega_s{}^2,\\
&V_3 = 2\ \zeta_s q\omega_s + q^2 + \omega_s{}^2 \quad \text{and} \quad V_4 = 2\ q\omega_d\zeta_d\mu_d + q^2\mu_d + \mu_d\omega_d{}^2 + c_e q
\end{aligned}
\tag{5}
$$

The dynamic response of the top degree of freedom derives as

$$
Z_5(q) = \frac{X_5}{X_g} = \frac{\left(\begin{array}{c} -\left(q^4 + 5\ q^2\omega_s{}^2 + 5\ \omega_s{}^4\right)\left(q^2 + 3\ \omega_s{}^2\right)\\ \left(2\ \zeta_d q\omega_d\mu_d + \omega_d{}^2\mu_d + c_e q\right)\left(q^2 + \omega_s{}^2\right)\end{array}\right)}{\Delta_b} \tag{6}
$$

The dynamic response of the isolators derives as

$$Z_b(q) = \frac{X_b}{X_g} = \frac{\begin{pmatrix} -q^{10}\mu_d - 9\ q^8\mu_d{\omega_s}^2 - 28\ q^6\mu_d{\omega_s}^4 - 35\ q^4\mu_d{\omega_s}^6 \\ -15\ q^2\mu_d{\omega_s}^8 - \mu_d{\omega_s}^{10} - q^8{\omega_s}^2 - 8\ q^6{\omega_s}^4 - 21\ q^4{\omega_s}^6 \\ -20\ q^2{\omega_s}^8 - 5\ {\omega_s}^{10} \end{pmatrix}}{\Delta_b} \tag{7}$$

The denominator Δ_b obtains

$$\begin{aligned} \Delta_b = {} & q^{12}\mu_d + (2\ \zeta_d\mu_d\omega_d + c_e)q^{11} + \left({\omega_d}^2\mu_d + 9\ {\omega_s}^2\mu_d + {\omega_s}^2\right)q^{10} \\ & + \left(18\ \zeta_d{\omega_s}^2\omega_d\mu_d + 9\ c_e{\omega_s}^2\right)q^9 + \left(9\ \mu_d{\omega_d}^2{\omega_s}^2 + 28\ {\omega_s}^4\mu_d + 8\ {\omega_s}^4\right)q^8 \\ & + \left(56\ \zeta_d{\omega_s}^4\omega_d\mu_d + 28\ c_e{\omega_s}^4\right)q^7 + \left(28\ \mu_d{\omega_d}^2{\omega_s}^4 + 35\ {\omega_s}^6\mu_d + 21\ {\omega_s}^6\right)q^6 \\ & + \left(70\ \zeta_d{\omega_s}^6\omega_d\mu_d + 35\ c_e{\omega_s}^6\right)q^5 + \left(35\ \mu_d{\omega_d}^2{\omega_s}^6 + 15\ {\omega_s}^8\mu_d + 20\ {\omega_s}^8\right)q^4 \\ & + \left(30\ \zeta_d{\omega_s}^8\omega_d\mu_d + 15\ c_e{\omega_s}^8\right)q^3 + \left(15\ \mu_d{\omega_d}^2{\omega_s}^8 + \mu_d{\omega_s}^{10} + 5\ {\omega_s}^{10}\right)q^2 \\ & + \left(2\ \zeta_d{\omega_s}^{10}\omega_d\mu_d + c_e{\omega_s}^{10}\right)q + \mu_d{\omega_d}^2{\omega_s}^{10} \end{aligned} \tag{8}$$

3. H_2 optimization

H_2 optimization method applies to derive the exact closed-form expressions for optimal design parameters of the isolators [13, 24]. $\zeta_s = 0$ is considered, Eq. (8) is a 12^{th} order polynomial equation, and the standard deviation [13] of the dynamic response of the top DOF obtains

$$\sigma_{x_5}^2 = \frac{S_0\pi\ \omega_d\left(220\ {\zeta_d}^2\mu_d{\omega_s}^2 + 671\ \mu_d{\omega_d}^2 + 225\ {\omega_s}^2\right)}{2{\omega_s}^6\zeta_d} \tag{9}$$

The standard deviation for the isolator's dynamic responses derives as

$$\sigma_{x_b}^2 = \frac{S_0\pi\ \left({\mu_d}^2{\omega_s}^2 + 55\ \mu_d{\omega_b}^2 + 10\ \mu_d{\omega_s}^2 + 25\ {\omega_s}^2\right)}{2{\mu_d}^2{\omega_s}^2\zeta_b{\omega_b}^3} \tag{10}$$

To derive optimal design parameters, the mathematical formulations are the following:

$$\frac{\partial\sigma_{x_5}^2}{\partial\zeta_d} = 0 \quad \text{and} \quad \frac{\partial\sigma_{x_5}^2}{\partial\omega_d} = 0 \tag{11}$$

Equation (9) is placed in the first equation of Eq. (11); hence, the damping ratio of isolators is obtained.

$$\zeta_d = \frac{\sqrt{55}\sqrt{\mu_d(671\ \mu_d{\omega_d}^2 + 225\ {\omega_s}^2)}}{110\ \mu_d\omega_s} \tag{12}$$

Equation (12) substitutes in Eq. (13) which provides

$$\sigma_{x_5}^2 = \frac{S_0\pi\ \omega_d\left(1342\ \mu_d{\omega_b}^2 + 450\ {\omega_s}^2\right)\sqrt{55}\mu_d}{{\omega_s}^5\sqrt{\mu_d(671\ \mu_d{\omega_d}^2 + 225\ {\omega_s}^2)}} \tag{13}$$

Equation (13) places in the second equation of Eq. (11); hence, the optimal natural frequency of the isolators is obtained.

$$(\omega_d)_{\text{opt}} = \frac{15\omega_s}{\sqrt{1342\ \mu_d}} \tag{14}$$

Equation (14) is placed in Eq. (12); hence, the optimal damping ratio is derived as

$$(\zeta_d)_{\text{opt}} = \sqrt{\frac{45}{88\mu_d}} \tag{15}$$

Figure 2(a) illustrates the differences in the optimal frequency ratio of the isolators for different inertial angle values. As base mass increases, the optimal frequency ratio decreases but increases as the inertial angle increases. The optimal viscous damping ratio variations for isolators with different inertial angle values are depicted in Figure 2(b). As the base mass increases, the optimal viscous damping ratio decreases and increases as the inertial angle increases. An algorithm for detailed design procedure of optimum NIARFBI and NIAFPS for MDOF systems has been displayed in Figure 3. An algorithm for determining dynamic response reduction capacity of optimum NIARFBI and NIAFPS for MDOF systems has been displayed in Figure 4. The mathematical formulation to derive the dynamic response reduction capacity of NIARFBI and NIAFPS for the MDOF system is derived and expressed as

$$\begin{aligned} R_{NIARFBI}(\%) &= \left(\frac{H_{TBI} - H_{NIARFBI}}{H_{TBI}}\right) \times 100 \quad \text{and} \\ R_{NIAFPS}(\%) &= \left(\frac{H_{TBI} - H_{NIAFPS}}{H_{TBI}}\right) \times 100 \end{aligned} \tag{16}$$

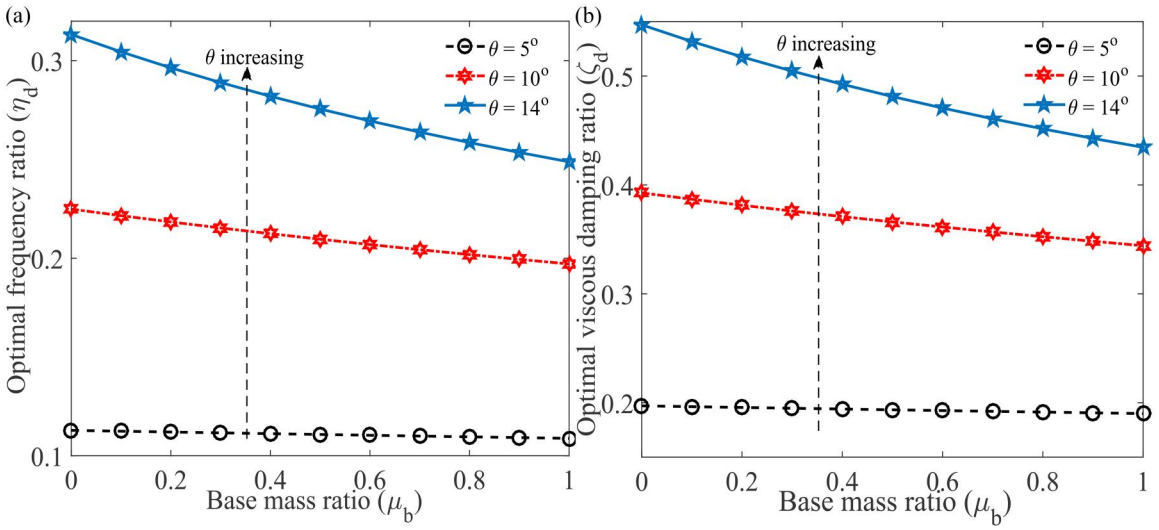

Figure 2. The variations of optimal (a) frequency ratio and (b) viscous damping ratio versus base mass ratio for different values of inertial angles.

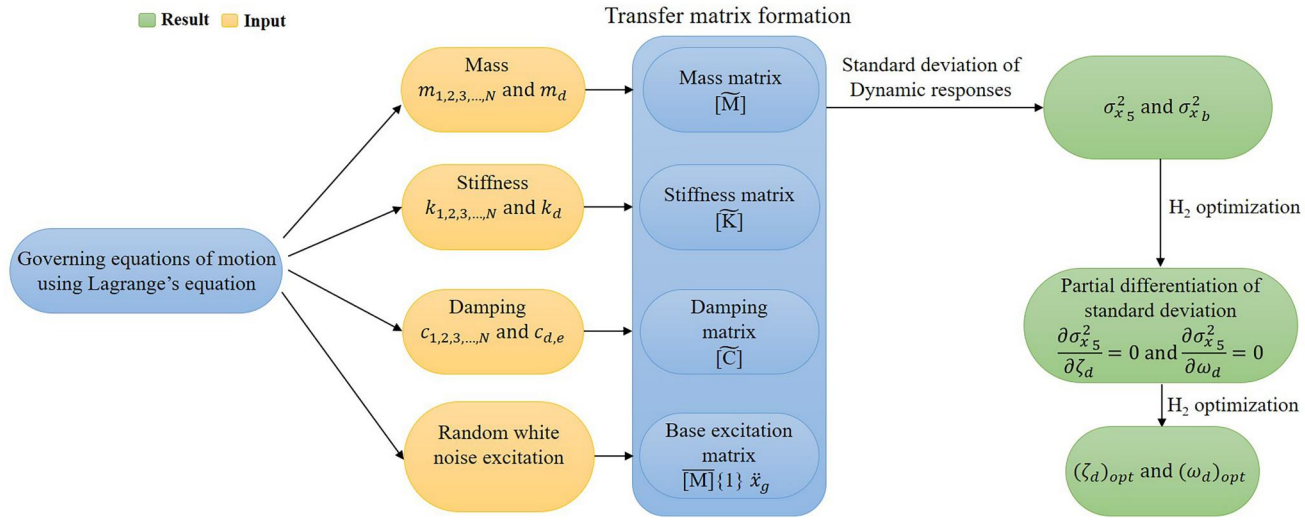

Figure 3. An algorithm for detailed design procedure of optimum NIARFBI and NIAFPS for MDOF systems.

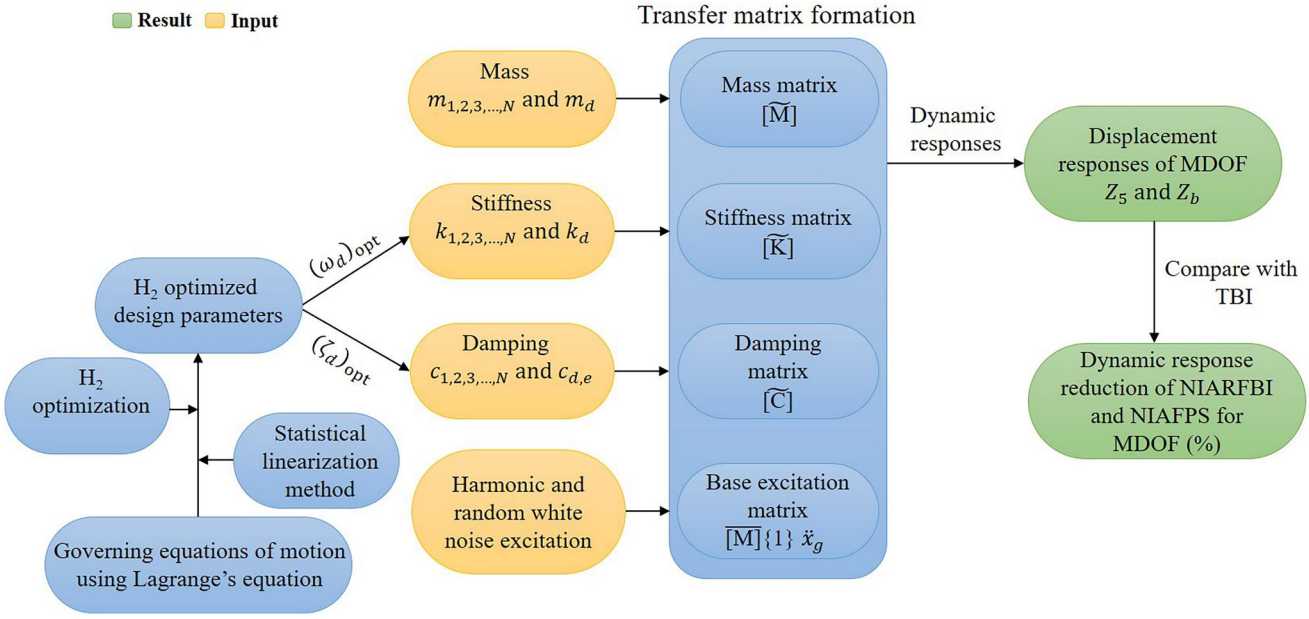

Figure 4. An algorithm for determining dynamic response reduction capacity of optimum NIARFBI and NIAFPS for MDOF systems.

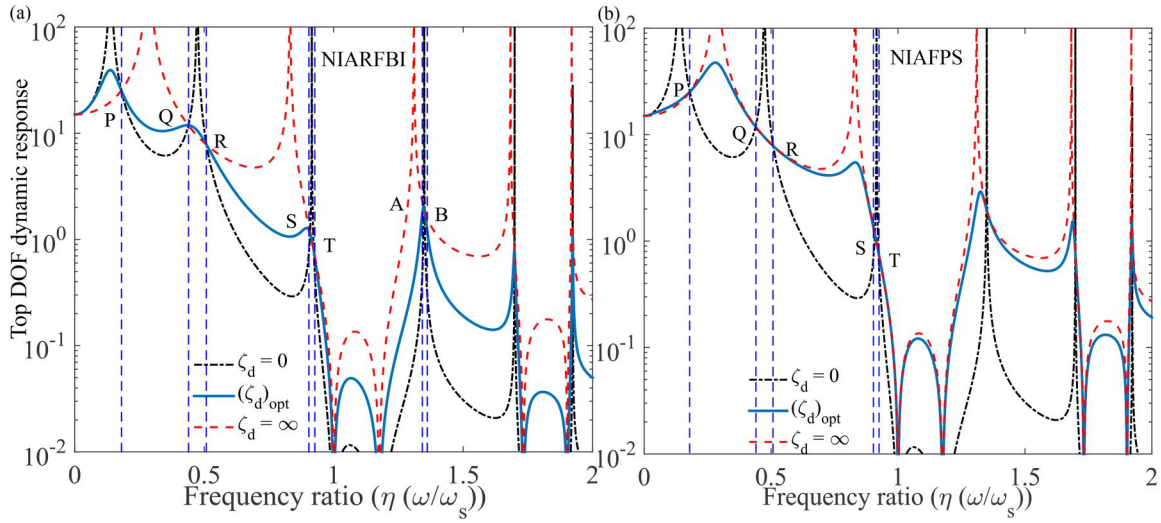

Figure 5. The variations of the optimal dynamic responses of the MDOF systems isolated (a) NIARFBI and (b) NIAFPS subjected to harmonic excitations.

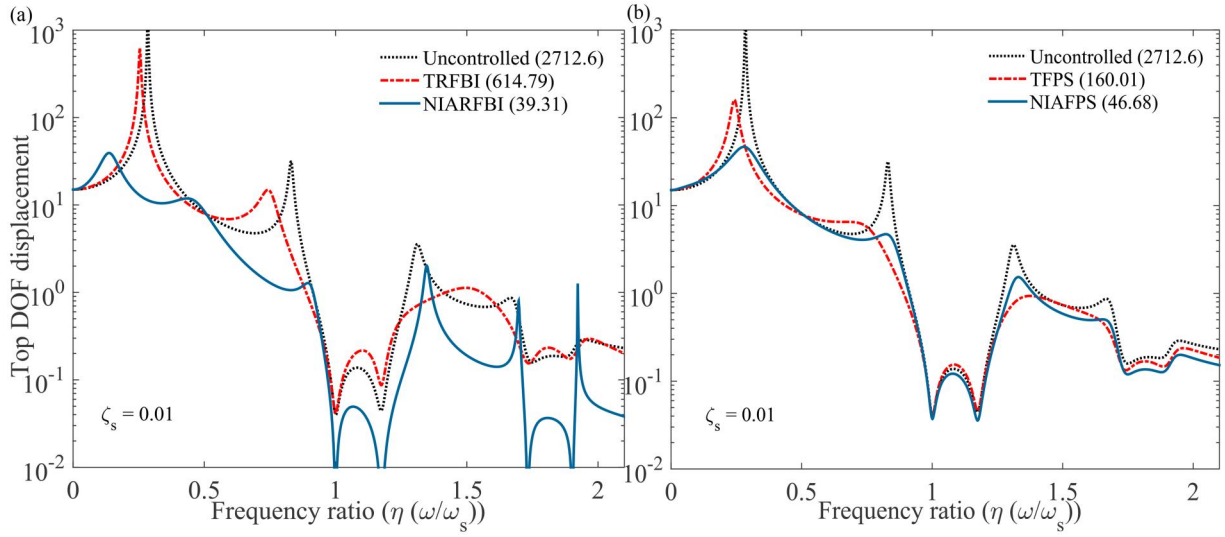

Figure 6. The variations of the top DOF's optimal displacement of the multiple degrees of freedom systems isolated (a) NIARFBI and (b) NIAFPS subjected to harmonic excitations.

Table 1. H_2 optimized system parameters for isolators.

		H_2 optimization		
System	Proposed by	η_d	ζ_d	μ
Novel nonlinear base isolators	This study	0.2638	0.4608	0.04
TRFBI	Matsagar and Jangid [25]	0.5	0.1	0.04
TFPS	R S Jangid [26]	0.4	0.1	0.05

TBI: base mass ratio (μ_B) = 1.1, Novel nonlinear base isolators: Total isolator mass ratio ($\mu_d = \mu_b + 2m_a$) = $0.7 + 2 \times 0.2 = 1.1$, Total mass ratio: $\mu_d = \mu_B$.

Table 2. System parameters of main structures (uncontrolled and controlled structures).

Name	Symbol	Values
Damping ratio	ζ_s	0.01

where $R_{NIARFBI}(\%)$ and R_{NIAFPS} are the dynamic response reduction capacities of NIARFBI and NIAFPS. H_{TBI}, $H_{NIARFBI}$, and H_{NIAFPS} are the maximum dynamic responses of the main structure's each degree of freedom (DOF).

4. Dynamic response evaluation

The variations of optimal top DOF's displacement of the MDOF system isolated by NIARFBI versus frequency ratio are shown in Figure 5(a). At $\zeta_d = 0$, Eigen frequencies locates in $\eta = 0.1382$, 0.4732, 0.9154, 1.349, 1.699, and 1.919. At $(\zeta_d)_{\text{opt}}$, resonating frequencies locates in $\eta =$ 0.1371, 0.435, 0.8948, 1.348 and 1.698. The superstructural frequency peaks locate at $\zeta_d = \infty$, i.e. $\eta = 0.2846$, 0.8308, 1.31, 1.683, and 1.919. The variations of optimal displacement of the MDOF system isolated by NIAFPS versus frequency ratio are shown in Figure 5(b). At $\zeta_d = 0$, Eigen frequencies locates in $\eta = 0.1382$, 0.4732, 0.9154, 1.349, 1.699, and 1.923. At $(\zeta_d)_{\text{opt}}$, resonating frequencies locates in $\eta = 0.28$, 0.8311, 1.325, 1.688, and 1.921. The superstructural frequency peaks locate at $\zeta_d = \infty$, i.e. $\eta = 0.2846$, 0.8308, 1.31, 1.683, and 1.919. The variations of the optimal top DOF's displacement of the MDOF systems isolated NIARFBI and TRFBI subjected to harmonic excitations have been shown in Figure 6(a). The optimal design parameters for novel nonlinear isolators and traditional base isolators (TBI) [25] are listed in Table 1. The mass ratio for novel and traditional isolators is taken at 1.1. The damping ratio of each degree of freedom is taken at 0.01 and $\mu = 0.04$. The system parameter for each degree of freedom is listed in Table 2. The system parameters for novel nonlinear isolators are considered as $\mu_b = 0.7, \mu_a = 0.2, (\zeta_d)_{\text{opt}} = 0.4608, (\eta_d)_{\text{opt}} = 0.2638, \theta = 14^o$, and $\mu = 0.04$. The structure's damping ratio is $\zeta_s = 0.01$. The maximum displacement of the uncontrolled structures' top degree of freedom (DOF) is determined as 2712.6. The maximum displacements of the top DOF of the MDOF system isolated by TRFBI and NIARFBI are determined as 614.79 and 39.31. The displacement reduction capacity of optimum NIARFBI is significantly 93.60% superior to TRFBI. The variations of the optimal displacements of the MDOF systems isolated NIAFPS and TFPS subjected to harmonic excitations have been shown in Figure 6(b). The maximum displacements of the top DOF of the MDOF system isolated by TFPS and NIAFPS are determined as 160.01 and 46.68. The displacement reduction capacity of optimum NIAFPS is significantly 70.82% superior to TFPS. The variations of the optimal displacements of the MDOF isolated by NIARFBI and TRFBI subjected to random-white excitations have been shown in Figure 7(a). The maximum displacement of the top DOF of the uncontrolled structures is determined as 5.95×10^10 dB/Hz. The maximum displacements of the top DOF of the structures isolated by TRFBI and NIARFBI are determined

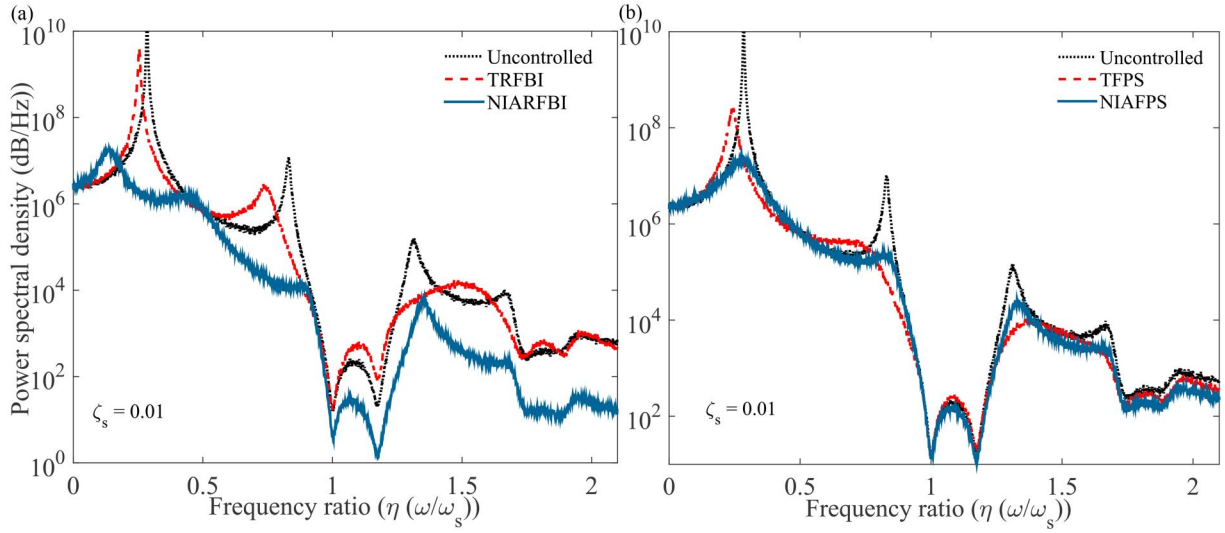

Figure 7. The variations of the optimal displacement of the MDOF system isolated (a) NIARFBI and (b) NIAFPS subjected to random-white noise.

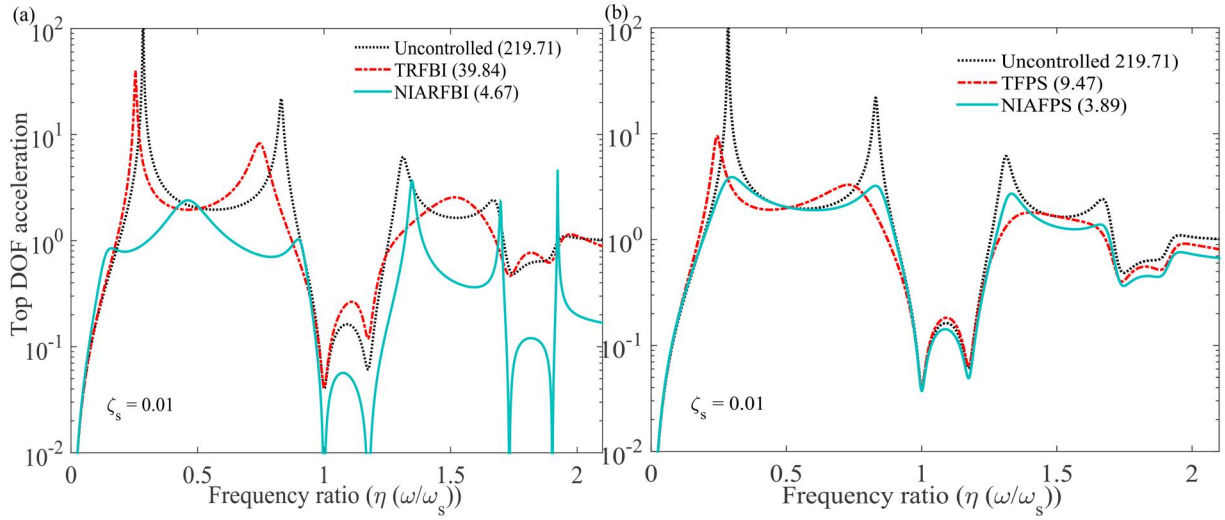

Figure 8. The variations of the top DOF's optimal accelerations of the multiple degrees of freedom systems isolated (a) NIARFBI and (b) NIAFPS subjected to harmonic excitations.

as 4.08×10^9 dB/Hz and 1.94×10^7 dB/Hz. The displacement reduction capacity of optimum NIARFBI is significantly 99.52% superior to TRFBI. The variations of the optimal displacements of the MDOF system isolated NIAFPS and TFPS subjected to random-white excitations have been shown in Figure 7(b). The maximum displacement of the top floor of the uncontrolled structures is determined as 5.8828×10^10 dB/Hz. The maximum displacements of the top floor of the structures isolated by TFPS and NIAFPS are determined as 2.96×10^8 dB/Hz and 2.50×10^7 dB/Hz. The displacement reduction capacity of optimum NIAFPS is significantly 91.52% superior to TFPS. The variations of the optimal accelerations of the MDOF systems isolated NIARFBI and TRFBI subjected to harmonic excitations have been shown in Figure 8(a). The maximum acceleration of the uncontrolled structures' top degree of freedom (DOF) is determined as 219.71. The maximum accelerations of the top DOF of the MDOF system isolated by TRFBI and NIARFBI are determined as 39.84 and 4.67. The acceleration reduction capacity of optimum NIARFBI is significantly 88.27% superior to TRFBI. The variations of the optimal accelerations of the MDOF systems isolated NIAFPS and TFPS subjected to harmonic excitations have been shown in Figure 8(b). The maximum displacements of the top DOF of the MDOF system isolated by TFPS and NIAFPS are determined as 9.47 and 3.89. The displacement reduction capacity of optimum NIAFPS is significantly 58.92% superior to TFPS. The variations of the optimal displacement of isolation level of the MDOF systems isolated NIARFBI and TRFBI subjected to harmonic excitations have been shown in Figure 9(a). The maximum displacement of isolation level of the MDOF system isolated by TRFBI and NIARFBI are determined as 124.03 and 91.12. The displacement reduction capacity of optimum NIARFBI in terms of maximum displacement of isolation level is significantly 26.53% superior to TRFBI. The variations of the optimal displacement of isolation level of the MDOF systems isolated NIAFPS and TFPS subjected to harmonic excitations

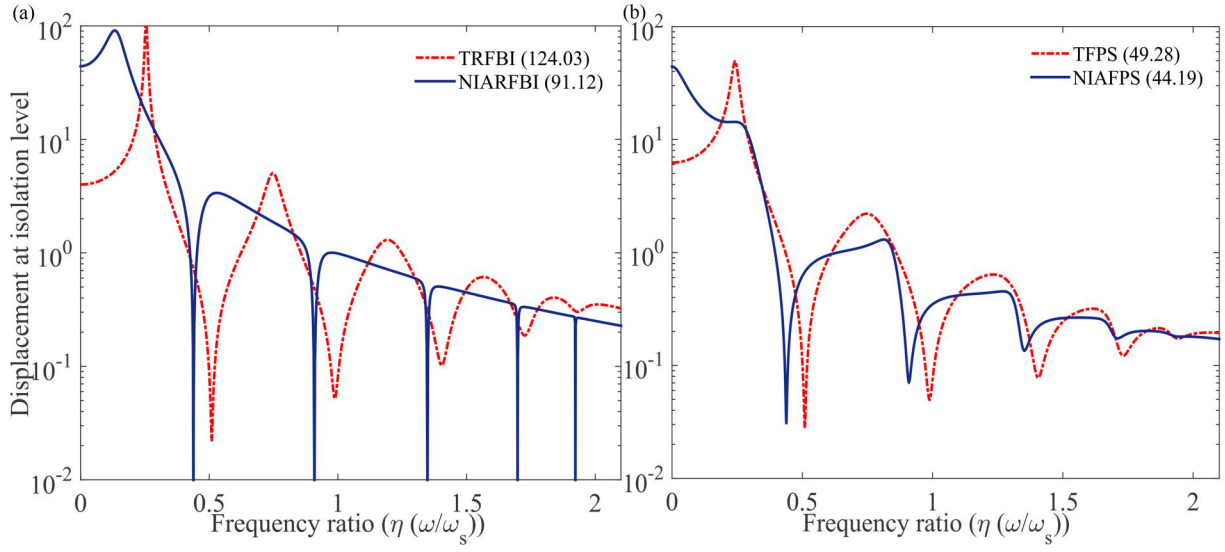

Figure 9. The variations of the top DOF's optimal displacement of isolation level of the multiple degrees of freedom systems isolated (a) NIARFBI and (b) NIAFPS subjected to harmonic excitations.

have been shown in Figure 9(b). The maximum displacement of isolation level of the MDOF system isolated by TFPS and NIAFPS are determined as 49.28 and 44.19. The displacement reduction capacity of optimum NIAFPS in terms of maximum displacement of isolation level is significantly 10.32% superior to TFPS.

5. Summary and conclusions

The fundamental innovation of this research is the introduction of the NIARFBI and NIAFPS and their accompanying optimum design parameters employing H_2 optimization techniques. A parametric study is carried out using these optimized design parameters. The optimal frequency ratio decreases with the base mass ratio but increases with the inertial angle. The optimal viscous damping ratio reduces as base mass increases and increases as the inertial angle increases. The displacement reduction capacity of optimum NIARFBI is significantly 93.60% and 99.52%, superior to TRFBI subjected to harmonic and random white noise excitations. The displacement reduction capacity of optimum NIAFPS is significantly 70.82% and 91.52%, superior to TFPS subjected to harmonic and random white noise excitations. The acceleration reduction capacities of optimum NIARFBI and NIAFPS are 88.27% and 58.92% superior to TRFBI and TFPS. The displacement reduction capacities of optimum NIARFBI and NIAFPS in terms of maximum displacement of isolation level are 26.53% and 10.32%, superior to TRFBI and TFPS. The conceptualization of NIARFBI, NIAFPS, and the accompanying optimum closed-form solutions is the paper's key original contribution. After using these closed-form formulas for the optimal design parameters, the robust dynamic response reduction capacity of the optimal NIARFBI and NIAFPS is achieved. Future studies may focus on using proposed isolators to bridges to reduce vibration.

Disclosure statement

The authors declare that they have no known competing financial interests or personal relationships that could have appeared to influence the work reported in this paper.

Funding

The authors would like to acknowledge the Inspire faculty grant, grant number DST/INSPIRE/04/2018/000052 for partial financial support for the project. SC would like to acknowledge the MHRD grant received from IIT Delhi during the period of this research work.

ORCID

Sudip Chowdhury http://orcid.org/0000-0001-6218-4843
Arnab Banerjee http://orcid.org/0000-0002-3157-6200
Sondipon Adhikari http://orcid.org/0000-0003-4181-3457

Data availability statement

All data, models, and code generated or used during the study appear in the submitted article.

References

[1] A. Carotti, and F. De Miranda, Passive antiseismic protections of multistorey building by controlled buckling of a steel base-isolation system, Mech. Res. Commun., vol. 17, no. 3, pp. 149–155, 1990. DOI: 10.1016/0093-6413(90)90043-C.

[2] C. Masnata, A. Di Matteo, C. Adam, and A. Pirrotta, Nontraditional configuration of tuned liquid column damper inerter for base-isolated structures, Mech. Res. Commun., vol. 129, pp. 104101, 2023. DOI: 10.1016/j.mechrescom.2023.104101.

[3] C. Masnata, A. Di Matteo, C. Adam, and A. Pirrotta, Smart structures through nontraditional design of tuned mass damper inerter for higher control of base isolated systems, Mech. Res. Commun., vol. 105, pp. 103513, 2020. DOI: 10.1016/j.mechrescom.2020.103513.

[4] G. Quaranta, G. Angelucci, and F. Mollaioli, Near-fault earthquakes with pulse-like horizontal and vertical seismic ground

motion components: analysis and effects on elastomeric bearings, Soil Dyn. Earthquake Eng., vol. 160, pp. 107361, 2022. DOI: 10.1016/j.soildyn.2022.107361.

[5] G. Shi, X. Yu, H. Meng, F. Zhao, J. Wang, J. Jiao, and H. Jiang, Effect of surface modification on friction characteristics of sliding bearings: a review, Tribol. Int., vol. 177, pp. 107937, 2023. DOI: 10.1016/j.triboint.2022.107937.

[6] J. Sun, and G. Zhufu, Mechanical behavior of laminated rubber isolation bearing with buckling steel plate, Int J Steel Struct., vol. 22, no. 4, pp. 1069–1085, 2022. DOI: 10.1007/s13296-022-00623-0.

[7] X. Chen, K. Ikago, Z. Guan, J. Li, and X. Wang, Lead-rubber-bearing with negative stiffness springs (lrb-ns) for base-isolation seismic design of resilient bridges: a theoretical feasibility study, Eng. Struct., vol. 266, pp. 114601, 2022. DOI: 10.1016/j.engstruct.2022.114601.

[8] S. Chowdhury, A. Banerjee, and S. Adhikari, The optimal configuration of negative stiffness inerter-based base isolators in multi-storey buildings, Structures, vol. 50, pp. 1232–1251, 2023. DOI: 10.1016/j.istruc.2023.02.095.

[9] S. Chowdhury, A. Banerjee, and S. Adhikari, The optimum inertial amplifier viscoelastic base isolators for dynamic response mitigation of structures: an analytical study, J. Struct. Integr. Maint., vol. 8, no. 3, pp. 150–160, 2023. DOI: 10.1080/24705314.2023.2176619.

[10] S. Wen, J. Jing, D. Cui, Z. Wu, W. Liu, and F. Li, Vibration isolation of a double-layered stewart platform with local oscillators, Mech. Adv. Mater. Struct., vol. 29, no. 27, pp. 6685–6693, 2022. DOI: 10.1080/15376494.2021.1983896.

[11] Z.-H. He, Z.-D. Xu, J.-Y. Xue, X.-J. Jing, Y.-R. Dong, and Q.-Q. Li, Experimental and mathematical model of a novel viscoelastic bio-inspired multi-dimensional vibration isolation device, Mech. Adv. Mater. Struct., pp. 1–17, 2022. DOI: 10.1080/15376494.2022.2132434.

[12] X. Liang, and J. Yuan, An absolute-zero-stiffness vibration isolator for continuously varying mass: theoretical design and numerical simulation, Mech. Adv. Mater. Struct., pp. 1–15, 2023. DOI: 10.1080/15376494.2023.2211408.

[13] S. Chowdhury, and A. Banerjee, The exact closed-form expressions for optimal design parameters of resonating base isolators, Int. J. Mech. Sci., vol. 224, pp. 107284, 2022. DOI: 10.1016/j.ijmecsci.2022.107284.

[14] Y. Wang, H.-X. Li, W.-A. Jiang, H. Ding, and L.-Q. Chen, A base excited mixed-connected inerter-based quasi-zero stiffness vibration isolator with mistuned load, Mech. Adv. Mater. Struct., vol. 29, no. 25, pp. 4224–4242, 2022. DOI: 10.1080/15376494.2021.1922961.

[15] Y. Chen, J. Xu, Y. Tai, X. Xu, and N. Chen, Critical damping design method of vibration isolation system with both fractional-order inerter and damper, Mech. Adv. Mater. Struct., vol. 29, no. 9, pp. 1348–1359, 2022. DOI: 10.1080/15376494.2020.1819490.

[16] M.C. Smith, Synthesis of mechanical networks: the inerter, IEEE Trans. Automat. Contr., vol. 47, no. 10, pp. 1648–1662, 2002. DOI: 10.1109/TAC.2002.803532.

[17] L. Cao, and C. Li, A high performance hybrid passive base-isolated system, Struct. Contr. Health, vol. 29, no. 3, pp. e2887, 2022. DOI: 10.1002/stc.2887.

[18] C. Li, K. Chang, L. Cao, and Y. Huang, Performance of a nonlinear hybrid base isolation system under the ground motions, Soil Dyn. Earthquake Eng., vol. 143, pp. 106589, 2021. DOI: 10.1016/j.soildyn.2021.106589.

[19] S. Adhikari, and A. Banerjee, Enhanced low-frequency vibration energy harvesting with inertial amplifiers, J. Intell. Mater. Syst. Struct., vol. 33, no. 6, pp. 822–838, 2022. DOI: 10.1177/1045389X211032281.

[20] D. Mu, K. Wang, H. Shu, and J. Lu, A two-stage inertial amplification tuned mass damper with grounded stiffness element, Mech. Adv. Mater. Struct., vol. 30, no. 19, pp. 3885–3896, 2023. DOI: 10.1080/15376494.2022.2084801.

[21] F. Fulton, and V.S. Sorokin, Analysis of the effects of nonlinear damping on a multiple-degree-of-freedom quasi-zero-stiffness vibration isolator, Mech. Res. Commun., vol. 130, pp. 104121, 2023. DOI: 10.1016/j.mechrescom.2023.104121.

[22] J.B. Roberts, and P.D. Spanos, Random Vibration and Statistical Linearization, Dover publications, Inc Mineola, New York, 2003.

[23] S. Chowdhury, and A. Banerjee, The nonlinear dynamic analysis of optimum nonlinear inertial amplifier base isolators for vibration isolation, Nonlinear Dyn., vol. 111, no. 14, pp. 12749–12786, 2023. DOI: 10.1007/s11071-023-08599-0.

[24] S. Chowdhury, A. Banerjee, and S. Adhikari, Optimal negative stiffness inertial-amplifier-base-isolators: exact closed-form expressions, Int. J. Mech. Sci., vol. 218, pp. 107044, 2022. DOI: 10.1016/j.ijmecsci.2021.107044.

[25] V.A. Matsagar, and R. Jangid, Seismic response of base-isolated structures during impact with adjacent structures, Eng. Struct., vol. 25, no. 10, pp. 1311–1323, 2003. DOI: 10.1016/S0141-0296(03)00081-6.

[26] R. Jangid, Optimum friction pendulum system for near-fault motions, Eng. Struct., vol. 27, no. 3, pp. 349–359, 2005. DOI: 10.1016/j.engstruct.2004.09.013.